

## Improving Transparency in Delay-free and Delayed Teleoperation: A Generalized 4-Channel Control Architecture

A. Aziminejad<sup>†‡</sup>, M. Tavakoli<sup>\*</sup>, R.V. Patel<sup>†‡</sup>, M. Moallem<sup>§</sup>

<sup>†</sup> Department of Electrical and Computer Engineering, University of Western Ontario,  
London, ON, N6A 5B9, Canada

<sup>‡</sup> Canadian Surgical Technologies & Advanced Robotics, 339 Windermere Road,  
London, ON, N6A 5A5, Canada

<sup>\*</sup> School of Engineering & Applied Sciences, Harvard University, 60 Oxford Street,  
Cambridge, MA, 02138, USA

<sup>§</sup> School of Engineering Science, Simon Fraser University Surrey, 250-13450 102nd Avenue,  
Surrey, BC, V3T 0A3, Canada

aazimin@uwo.ca, tavakoli@seas.harvard.edu, rajni@eng.uwo.ca, mmoallem@sfu.ca

**Abstract**—In master-slave teleoperation applications that deal with a delicate and sensitive environment, it is important to provide high-fidelity haptic feedback of slave/environment interactions to the user's hand. For haptic teleoperation, in addition to a haptics-capable master interface, often one or more force sensors are also used, which warrant new bilateral control architectures while increasing the cost and complexity of the teleoperation system. In this paper, considering a four-channel architecture, we investigate the added benefits of using force sensors that measure hand/master and slave/environment interactions and utilizing local feedback loops on teleoperation transparency. Furthermore, we propose a novel method for incorporating wave transformation delay compensation technique in the four-channel architecture, which is the best architecture for providing transparency. It is demonstrated that the proposed teleoperation architecture is capable of providing absolute stability as well as ideal transparency under time delay and the corresponding conditions for each of these two operation modes have been derived. Experimental results in support of the developed theory are provided.

**Index Terms**—Bilateral teleoperation control, transparency, passivity, wave transformation, haptics.

### 1. INTRODUCTION

A master-slave teleoperation system consists of a slave robot and a master human-machine interface (HMI) from which the human operator controls the slave and is provided with visual feedback from the slave side. In teleoperation applications that deal with a delicate and sensitive environment such as soft-tissue

surgery, it is important to also provide feedback of slave/environment contact forces (haptic feedback) to the user's hand. Such feedback is shown to enhance human performance [1].

The first issue addressed in this paper (Section 3) is the extent of benefits added by two force sensors and the effects of the resulting 4-channel (4CH) bilateral control structure on teleoperation stability and transparency, which can be compromised due to implementation issues and changes in the environment dynamics. We also study the effect of local force feedback loops in terms of improving the robustness of teleoperation system stability and performance against time delays in a teleoperation system.

Scattering approaches which inherently preserve passivity are theoretically able to stabilize a teleoperation system independent of transmission delays [2]. A more physically motivated reformulation of these ideas led to the introduction of wave theory [3], which provides a framework for designing and analyzing bilateral teleoperation systems. However, so far these concepts have only been applied to a two-channel (2CH) position error-based (PEB) teleoperation system. Having demonstrated the unrivalled advantage of the 4CH architecture from a transparency perspective for the delay-free condition, as the second issue addressed in this paper (Section 4), we extend wave theory in a manner which can be applied to the 4CH architecture, and compare the transparency of an optimized 4CH architecture and its less complex three-channel (3CH) variant with that of a 2CH architecture in terms of the

hybrid parameters of the equivalent two-port network.

Finally, in the experiments of Section 5, which were performed using a haptics-enabled master-slave testbed developed in our lab, the performance of the conventional and wave-based 4CH bilateral control architectures are investigated during soft-tissue palpation tests in order to validate the theoretical conclusions.

## 2. STABILITY AND TRANSPARENCY IN HAPTIC TELEOPERATION

For safe and precise teleoperation, stability and transparency of the master-slave system are essential. A teleoperation system is said to be stable if the state variables of the system are bounded at all times. When communication time delay is not involved, the stability analysis in a bilateral teleoperation system is straightforward. However, this issue becomes difficult when a communication time delay  $T$  is present, because a term  $e^{-sT}$  turns the finite-dimensional system to an infinite-dimensional one.

As a performance measure, Lawrence [4] has defined transparency as “the description of the degree of telepresence of the remote site available to the human operator through the teleoperator device”. Transparency of a bilaterally controlled teleoperator depends on how well the slave/environment interaction forces are reflected to the user’s hand by the master. Denoting the hand/master interaction as  $f_h$  and the slave/environment interaction as  $f_e$ , the dynamics of the master and the slave can be written as:

$$f_m + f_h = M_m \ddot{x}_m, \quad f_s - f_e = M_s \ddot{x}_s \quad (2.1)$$

where  $M_m$ ,  $M_s$ ,  $x_m$ ,  $x_s$ ,  $f_m$  and  $f_s$  are the master and the slave inertias, positions and control signals (force or torque), respectively. In an ideally transparent teleoperation system, through appropriate control signals  $f_m$  and  $f_s$ , the master and the slave positions and interactions will match regardless of the operator and environment dynamics:

$$x_m = x_s, \quad f_h = f_e \quad (2.2)$$

By considering velocities and forces in a teleoperation system as currents and voltages, an equivalent circuit representation of the system can be obtained [5] (Figure 2.1), in which impedances  $Z_h(s)$  and  $Z_e(s)$  denote dynamic characteristics of the human operator’s hand and the remote environment, respectively. Here,

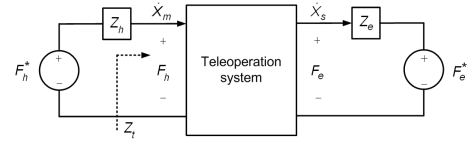


Fig. 2.1. Equivalent circuit representation of a teleoperation system.

$F_h^*$  and  $F_e^*$  are respectively the operator’s and the environment’s exogenous input forces and are independent of teleoperation system behavior. It is generally assumed that the environment is passive ( $F_e^* = 0$ ) and the operator is passive in the sense that he/she does not perform actions that will make the teleoperation system unstable.

To evaluate the transparency of teleoperation, the hybrid representation of the two-port network model of a master-slave system is most suitable. In this representation:

$$\begin{bmatrix} F_h \\ -\dot{X}_s \end{bmatrix} = \begin{bmatrix} h_{11} & h_{12} \\ h_{21} & h_{22} \end{bmatrix} \begin{bmatrix} \dot{X}_m \\ F_e \end{bmatrix} \quad (2.3)$$

Note that we have used velocities in the hybrid representation rather than positions. This convention does not affect stability and transparency, although it might possibly cause small offsets between master and slave positions (steady-state errors in positions or position drifts) [4]. From (2.2) and (2.3), perfect transparency is achieved if and only if the hybrid matrix has the following form

$$H_{\text{ideal}} = \begin{bmatrix} 0 & 1 \\ -1 & 0 \end{bmatrix} \quad (2.4)$$

Each element of the  $H$  matrix has a physical meaning. The hybrid parameter  $h_{11} = F_h/\dot{X}_m|_{F_e=0}$  is the input impedance in free-motion condition. Nonzero values for  $h_{11}$  mean that even when the slave is in free space, the user will receive some force feedback, thus giving a “sticky” feel of free-motion movements. The parameter  $h_{12} = F_h/F_e|_{\dot{X}_m=0}$  is a measure of force tracking for the haptic teleoperation system when the master is locked in motion (perfect force tracking for  $h_{12} = 1$ ). The parameter  $h_{21} = -\dot{X}_s/\dot{X}_m|_{F_e=0}$  is a measure of position (velocity) tracking performance when the slave is in free space (perfect position/velocity tracking for  $h_{21} = -1$ ). The parameter  $h_{22} = -\dot{X}_s/F_e|_{\dot{X}_m=0}$  is the output admittance when the master is locked in motion. Nonzero values for  $h_{22}$  indicate that even when the master is locked in place,

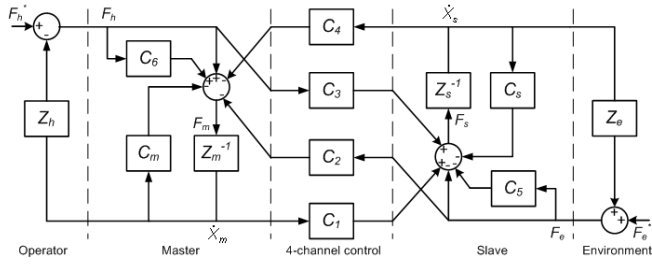


Fig. 3.1. 4CH bilateral teleoperation system without time delay.

the slave will move in response to slave/environment contacts.

### 3. DELAY-FREE 4CH ARCHITECTURE

For achieving the ideal delay-free response (2.4), various teleoperation control architectures are proposed in the literature. These control architectures are usually classified as position-force (i.e. position control at the master side and force control at the slave side), force-position, position-position, and force-force architectures. Among these four architectures, in order to have a stiff slave, we are interested in those in which the slave is under position control, namely position-position and force-position. A more general classification is by the number of communication channels required for transmitting position and force values from the master to the slave and vice versa in each bilateral control architecture. Under this classification, the above-mentioned control architectures are called two-channel (2CH). In this section, we discuss the stability and transparency of a 4CH architecture.

Figure 3.1 depicts a general 4-channel (4CH) bilateral teleoperation architecture [4], [6]. This architecture can represent other teleoperation structures through appropriate selection of subsystem dynamics  $C_1$  to  $C_6$ . The compensators  $C_5$  and  $C_6$  in Figure 3.1 constitute local force feedback at the slave side and the master side, respectively. The H-parameters for the 4CH architecture in Figure 3.1 are:

$$\begin{aligned} h_{11} &= (Z_{ts}Z_{tm} + C_1C_4)/D \\ h_{12} &= [Z_{ts}C_2 - (1 + C_5)C_4]/D \\ h_{21} &= -[Z_{tm}C_3 + (1 + C_6)C_1]/D \\ h_{22} &= -[C_2C_3 - (1 + C_5)(1 + C_6)]/D \end{aligned} \quad (3.1)$$

where  $D = -C_3C_4 + Z_{ts}(1 + C_6)$  and  $Z_{tm} = M_ms + C_m(s) = M_ms + k_{dm} + k_{pm}/s$  and  $Z_{ts} = M_ss + C_s(s) = M_ss + k_{ds} + k_{ps}/s$ .

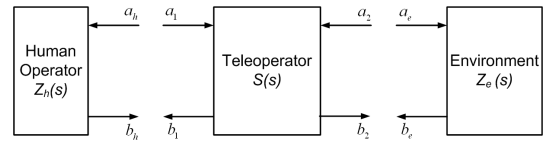


Fig. 3.2. A generalized description of a bilateral teleoperation system in terms of scattering parameters.

In contrast to the 2CH architectures, a sufficient number of parameters (degrees of freedom) in the 4CH architecture enables it to achieve ideal transparency. In fact, by selecting  $C_1$  through  $C_6$  according to

$$\begin{aligned} C_1 &= Z_{ts}, & C_2 &= 1 + C_6, \\ C_3 &= 1 + C_5, & C_4 &= -Z_{tm} \end{aligned} \quad (3.2)$$

the ideal transparency conditions (2.4) are fully met.

For analysis of stability, we need to use the scattering theory, which is a powerful tool for investigation of absolute stability in two-port networks. Figure 3.2 depicts a scattering matrix representation of a bilateral teleoperation system and is expressed by  $b = S(s)a$ . Here,  $a = [a_1 \ a_2]^T$  and  $b = [b_1 \ b_2]^T$  are respectively the input and output waves of the teleoperation system, and are related to equivalent voltages and currents as  $a = (F + n^2\dot{X})/2$  and  $b = (F - n^2\dot{X})/2$  where  $F = [F_h \ F_e]^T$ ,  $\dot{X} = [\dot{X}_m \ -\dot{X}_s]^T$ , and  $n$  is a scaling factor.

*Theorem 3.1:* The necessary and sufficient condition for stability in a reciprocal two-port network ( $S_{12} = S_{21}$ ) with an RHP-analytic scattering matrix  $S(s)$  that is terminated with a passive operator and a passive environment is [7]:

$$\bar{\sigma}[S(j\omega)] \leq 1 \quad (3.3)$$

where  $\bar{\sigma}$  represents the maximum singular value of  $S(j\omega)$ . In the case of a non-reciprocal two-port network, the passivity condition (3.3) is only a sufficient condition for stability.  $\diamond$

*Theorem 3.2:* The necessary and sufficient condition for absolute stability of the 4CH teleoperation system of Figure 3.1 under ideal transparency conditions is that all coefficients of polynomial

$$\begin{aligned} D &= C_3Z_{tm} + C_2Z_{ts} \\ &= (M_mC_3 + M_sC_2)s^2 + (k_{dm}C_3 + k_{ds}C_2)s \\ &\quad + k_{pm}C_3 + k_{ps}C_2 \end{aligned} \quad (3.4)$$

have the same sign.

*Proof:* In the 4CH architecture, when the ideal transparency condition set (3.2) holds, the hybrid matrix is

$$H = \begin{bmatrix} 0 & \frac{D}{D} \\ -\frac{D}{D} & 0 \end{bmatrix} \quad (3.5)$$

where  $D$  is found to be as given in (3.4). The above hybrid matrix corresponds to the following scattering matrix:

$$S = \begin{bmatrix} \frac{-D^2+D^2}{2D^2} & \frac{2D^2}{2D^2} \\ \frac{2D^2}{2D^2} & \frac{D^2-D^2}{2D^2} \end{bmatrix} \quad (3.6)$$

For scattering matrix  $S$  in (3.6) to be RHP-analytic,  $D$  has to be Hurwitz. The necessary and sufficient condition for  $D$  being Hurwitz is that all the coefficients have the same sign. In this case,  $S$  can be simplified to

$$S = \begin{bmatrix} 0 & 1 \\ 1 & 0 \end{bmatrix} \quad (3.7)$$

Both of the singular values of this matrix are equal to 1. Therefore, since under ideal transparency condition the system is reciprocal, according to (3.3), the system is absolutely stable iff all the coefficients in the polynomial  $D$  given in (3.4) have the same sign. ■

#### A. Stability and performance robustness

It should be noted that under ideal transparent conditions, i.e., when the singular values of  $S(s)$  are 1, the passivity (and stability) critically depends on exact implementation of control laws and having the exact dynamics of the master and the slave as any non-ideality might increase the maximum singular value beyond unity. Such a low stability margin can be explained by the trade-off that exists between stability and transparency in bilateral teleoperation [4], [8].

One of the non-idealities that exists in practice is the processing delay and communication latency between the master and the slave. In the presence of time delay  $T_d$ , in an ideally transparent bilateral teleoperation system,

$$H = \begin{bmatrix} 0 & e^{-sT_d} \\ -e^{-sT_d} & 0 \end{bmatrix}, \quad S = \begin{bmatrix} -\tanh(sT_d) & \operatorname{sech}(sT_d) \\ \operatorname{sech}(sT_d) & \tanh(sT_d) \end{bmatrix} \quad (3.8)$$

It can be shown that  $\bar{\sigma}(S)$  for this scattering matrix is unbounded, consequently this system cannot maintain stability for all passive operators and environments. However, when  $Z_h$  and  $Z_e$  are factored in the analysis,

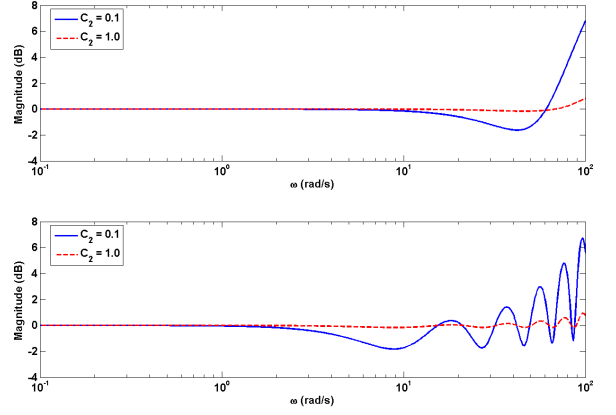


Fig. 3.3. The transparency transfer function magnitude for round-trip delays of  $T_d = 30$  msec (top) and  $T_d = 300$  msec (bottom).

the teleoperation system loses its reciprocity property and therefore, although not passive, it can be stabilized by proper choices of  $Z_h$  and  $Z_e$  [9].

In the 4CH architecture under time delay, when the ideal transparency condition set (3.2) holds, the operator's side transparency transfer function can be defined as

$$G_{op} = \frac{Z_t}{Z_e} \quad (3.9) \\ = \frac{Z_{tm}C_3 + Z_{ts}C_2e^{-2sT_d} + Z_{tm}Z_{ts}/Z_e(1 - e^{-2sT_d})}{Z_e(1 - e^{-2sT_d})C_3C_2 + Z_{ts}C_2 + Z_{tm}e^{-2sT_d}C_3}$$

Local force feedback terms  $C_5$  and  $C_6$  also help mitigate the undesirable effects of this non-ideality. It can easily be seen that in the absence of local force feedback terms ( $C_6 = C_2 - 1 = 0$ ,  $C_5 = C_3 - 1 = 0$ ),  $G_{op} \neq e^{-2sT_d}$ . However, with nonzero  $C_5$  and  $C_6$ , near-ideal transparency can be achieved. For instance, taking  $C_5 = -1$ , (3.9) will be reduced to  $G_{op} = e^{-2sT_d} + \frac{Z_{tm}}{Z_e C_2} (1 - e^{-2sT_d})$ , which approaches the ideal  $G_{op} = e^{-2sT_d}$  by selecting a sufficiently large  $C_2$ . To further illustrate this point, Figure 3.3 shows the magnitude of the frequency response of the transparency transfer function  $G_{op}$  for our experimental setup  $M_m$  and  $M_s$  (Section 5) with  $C_m(s) = M_m(80s + 1600)/s$ ,  $C_s(s) = M_s(80s + 1600)/s$ ,  $C_5 = -1$ , and one-way delays of  $T_d = 15$  msec (top) and  $T_d = 150$  msec (bottom). Evidently, with an increase in  $C_2$ , the magnitude of  $G_{op}$  nears 1 over a relatively wide frequency range.

#### B. 3CH case

Another potential benefit of the general 4CH architecture of Figure 3.1 is that by proper adjustment of the local feedback parameters, it is possible to obtain



delay. On the other hand, the characteristic equation of the transfer function from  $F'_h$  to  $V_m$  (or any other output in the system) can be calculated as

$$Z_{ts}(e^{2sT} - 1)/C_3 + Z_e e^{2sT} + Z_h = 0 \quad (4.4)$$

In order to obtain a necessary and sufficient condition for stability based on Routh-Hurwitz criterion, we use a second-order Pade approximation to re-write the characteristic equation (4.4) as

$$(3-3sT+s^2T^2)Z_hC_3+(3+3sT+s^2T^2)Z_eC_3+6sTZ_{ts} = 0 \quad (4.5)$$

Assuming  $Z_h = M_h s + k_{dh} + k_{ph}/s$  and  $Z_e = M_e s + k_{de} + k_{pe}/s$ , (4.5) involves a 4th-order polynomial in  $s$ . Application of Routh-Hurwitz theorem to (4.5) imposes an upper bound on  $C_3$  that is dependent on time delay  $T$ . However, such an upper bound on  $C_3$  for stability, limits transparency according to (4.3). Similarly, taking the 3CH architecture with  $C_3 = 0$  would lead to an upper bound on  $C_2$  for stability, which limits the transparency according to the operator's side transparency transfer function  $G_{op} = Z_t/Z_e$ . This fact provides the necessary incentive for extending the concept of passivity-based time delay compensation to the more flexible 4CH teleoperation architecture such that the system can remain stable at no penalty on transparency.

### C. Wave-Based 4CH Architecture

So far the passivity-based time delay compensation approach has been applied only to 2CH architectures. In order to extend this approach to a 4CH teleoperation architecture, we need to segregate the communication channel part of the system in Figure 3.1 as a two-port network. Figure 4.2 shows a possible method for accomplishing this extension. The non-physical input effort and flow pair for this two-port network model of the communication channel are

$$\begin{aligned} V_1 &= C_3 F_h + C_1 \dot{X}_m \\ I_2 &= C_2 F_e + C_4 \dot{X}_s \end{aligned} \quad (4.6)$$

The master and the slave closed-loop equations can be written as  $\dot{X}_m Z_m = -\dot{X}_m C_m + F_h(1 + C_6) - I_1$  and  $\dot{X}_s Z_s = -\dot{X}_s C_s - F_e(1 + C_5) + V_2$ . Therefore, the non-physical output flow and effort pair are

$$\begin{aligned} I_1 &= F_h(1 + C_6) - \dot{X}_m Z_{tm} \\ V_2 &= F_e(1 + C_5) + \dot{X}_s Z_{ts} \end{aligned} \quad (4.7)$$

The communication channel effort and flow relationships in (4.6) and (4.7), from which the input and output pseudo-power functions are calculated, are not unique but in their presented form they are independent of knowledge of  $Z_e$  and  $Z_h$ , which is an advantage for implementation. Moreover, it can be easily checked that for the case of  $T = 0$ ,  $V_1 = V_2$  and  $I_1 = I_2$ , thus the original system of Figure 3.1 is recovered. The communication channel can be modelled based on its inputs and outputs as

$$\begin{aligned} \begin{bmatrix} -I_1 \\ V_2 \end{bmatrix} &= \begin{bmatrix} c_{11} & c_{12} \\ c_{21} & c_{22} \end{bmatrix} \begin{bmatrix} V_1 \\ I_2 \end{bmatrix} \\ &= C(s) \begin{bmatrix} V_1 \\ I_2 \end{bmatrix} \end{aligned} \quad (4.8)$$

where the matrix  $C$  can be defined with respect to the hybrid matrix of the communication channel as

$$C(s) = H_{ch}^{-1}(s) \quad (4.9)$$

The outputs of the wave transformation block at the master side are

$$\begin{aligned} I_1 &= (\sqrt{2b}u_m - V_1)/b \\ v_m &= (bu_m - \sqrt{2b}V_1)/b \end{aligned} \quad (4.10)$$

and at the slave side are

$$\begin{aligned} V_2 &= bI_2 - \sqrt{2b}v_s \\ u_s &= \sqrt{2b}I_2 - v_s \end{aligned} \quad (4.11)$$

Transformation (4.10) can be derived from the basic definition of wave variables (i.e., equation (4.1)) by taking the flow variable ( $I_1$ ) and  $v_m$  as the outputs and the effort variable ( $V_1$ ) and  $u_m$  as the inputs. Similarly, wave transformation (4.11) is obtained from (4.2) through selecting  $V_2$  and  $u_s$  as the outputs and  $I_2$  and  $v_s$  as the inputs. This arrangement results from the fact that the input/output relationship for the communication channel of the proposed 4CH architecture corresponds to an ‘‘inverse hybrid’’ representation of a two-port network (i.e., its inputs are  $V_1$  and  $I_2$  and its outputs are  $-I_1$  and  $V_2$ , where the directions of the input and output flows correspond to the convention set in [2]) – see equation (4.9), whereas that relationship is in the form of a hybrid model for the 2CH architecture of Figure 4.1.

#### D. Transparency considerations and 3CH architecture

Applying condition set (3.2) for ideal transparency without time delay, the overall hybrid parameters of the proposed wave-based 4CH teleoperation system in Figure 4.2 are given by:

$$\begin{aligned} h_{11} &= [(W^2 e^{-2sT} - 1)(Z_{ts}^2 - b^2 Z_{tm}^2)]/D_2 \\ h_{12} &= 2bW e^{-sT} (Z_{tm} C_3 + Z_{ts} C_2)/D_2 \\ h_{21} &= -2bW e^{-sT} (Z_{tm} C_3 + Z_{ts} C_2)/D_2 \\ h_{22} &= [(W^2 e^{-2sT} - 1)(b^2 C_2^2 - C_3^2)]/D_2 \end{aligned} \quad (4.12)$$

where

$$\begin{aligned} D_2 &= b(W^2 e^{-2sT} + 1)(Z_{ts} C_2 + Z_{tm} C_3) \\ &+ (W^2 e^{-2sT} - 1)(-b^2 C_2 Z_{tm} - C_3 Z_{ts}) \end{aligned} \quad (4.13)$$

For asymptotic convergence of the position and torque errors in Figure 3.1, the controller gains should be chosen in accordance with [10] as:

$$C_s/C_m = M_s/M_m \quad (4.14)$$

Using (4.14), it can be easily shown that  $Z_{ts}/Z_{tm} = M_s/M_m$ . Setting  $h_{11}$  from (4.12) equal to zero under the ideal transparency condition according to (3.8) gives:

$$b_{\text{ideal}} = Z_{ts}/Z_{tm} \quad (4.15)$$

Similarly, for  $h_{22}$  to be equal to zero, we should have

$$C_3/C_2 = b_{\text{ideal}} \quad (4.16)$$

Using (4.15) and (4.16) in (4.12), expressions for  $h_{12}$  and  $h_{21}$  under ideal transparency condition can be derived as:

$$h_{12} = -h_{21} = W(s)e^{-sT} \quad (4.17)$$

Equation (4.17) means that for  $W(s) = 1$ , the condition set (3.2) along with equations (4.15) and (4.16) are delayed ideal transparency provisions for the proposed 4CH architecture of Figure 4.2.

It can be shown that a teleoperation system represented by the delayed ideally transparent hybrid matrix in (3.8) cannot preserve passivity [2]. Therefore, a stability study in this case also needs to factor  $Z_h$  and  $Z_e$ . For the teleoperation system under ideal transparency conditions, if  $Z_{ts}$  is Hurwitz ( $k_{ds}, k_{ps} > 0$ ), the input

admittance transfer function based on the input  $F'_h$  and the output  $\dot{X}_m$  can be simplified to

$$Y_{\text{in}} = (Z_h + Z_e e^{-2sT})^{-1} \quad (4.18)$$

In order to present a descriptive stability analysis of an ideally transparent delayed teleoperation system, it is possible to use Pade approximation to simplify the characteristic polynomial in (4.18) and apply the Routh-Hurwitz theorem assuming  $Z_h = (M_h s^2 + k_{dh} s + k_{ph})/s$  and  $Z_e = k_{pe}/s$ . For mathematical tractability, we use a first-order Pade approximation  $e^{-2sT} \simeq (1 - sT)/(1 + sT)$  to re-write the characteristic equation in (4.18) as

$$\begin{aligned} M_h T s^3 + (k_{dh} T + M_h) s^2 + \\ (-k_{ph} \alpha T + k_{ph} T + k_{dh}) s + k_{ph} \alpha + k_{ph} = 0 \end{aligned} \quad (4.19)$$

where  $\alpha = k_{pe}/k_{pm}$ . Applying Routh-Hurwitz theorem to (4.19), the following condition on  $\alpha$  as the necessary and sufficient condition for stability of the system represented by (4.18) will be derived

$$\alpha = \frac{k_{pe}}{k_{ph}} < \frac{k_{dh}(M_h + k_{dh} T + k_{ph} T^2)}{k_{ph}(2M_h + k_{dh} T) T} \quad (4.20)$$

Equation (4.20) sets an upper bound on the remote environment stiffness  $k_{pe}$  depending on the operator parameters and time delay. Generally speaking, condition (4.20) is easy to meet particularly under small delays or with compliant environments, or through operator's adaptation to the remote environment characteristics.

Deriving a wave-based 3CH architecture from the proposed wave-based 4CH architecture under ideal transparency provisions only affects  $h_{22}$ . In order to explain this further, assume under condition set (3.2) and provisions (4.14) and (4.15) that only the slave unity local force feedback is used (i.e.,  $C_5 = -1$  and  $C_6 = 0$ ). It can be easily shown that  $h_{11}$ ,  $h_{12}$ , and  $h_{21}$  still keep their ideal transparency values after this rearrangement. However, the new  $h_{22}$  is

$$h_{22} = (W^2 e^{-2sT} - 1)/(2Z_{tm}) \quad (4.21)$$

According to (4.21), the bigger the magnitude of  $Z_{tm}$ , the closer  $h_{22}$  is to its ideal value of zero. This result suggests that this 3CH architecture is suitable for applications in which the master is heavy. On the other hand, if only the master unity local force feedback is used (i.e.,  $C_6 = -1$  and  $C_5 = 0$ ), while  $h_{11}$ ,  $h_{12}$ ,

and  $h_{21}$  remain unchanged from their ideal transparency values, the new  $h_{22}$  is given by

$$h_{22} = (1 - W^2 e^{-2sT}) / (2Z_{ts}) \quad (4.22)$$

which shows that the second 3CH architecture is suitable for applications with a heavy slave robot.

## 5. HAPTIC TELEOPERATION EXPERIMENTS

### A. Experimental setup

For experimental evaluation of the different haptic teleoperation control methods described in Section 3 and 4, we used a bilateral master-slave system developed for endoscopic surgery experiments. Through a user interface (master), the user controls the motion of a surgical tool (slave) and receives force/torque feedback of the slave/tissue interactions. The developed master user interface is capable of providing the user with force feedback in all five DOFs available in endoscopic surgery (pitch, yaw, roll, insertion, and handle open/close) [11]. The developed slave endoscopic instrument is also capable of measuring interactions with tissue in all the five present DOFs [12]. In the experiments in this paper, the master and slave subsystems were constrained for force-reflective teleoperation in the twist direction only (i.e. rotations about the instrument axis). The digital control loop is implemented at a sampling frequency of 1000 Hz. The friction and gravity effects present in the master were determined and compensated for such that the user does not feel any weight on his/her hand when the slave is not in contact with an object. The friction-compensated master is represented as  $\tau_m = M_m \ddot{\theta}_m$  where  $M_m = 5.97 \times 10^{-4}$  kgm<sup>2</sup>. Using a similar method, the slave's model was identified as  $\tau_s = M_s \ddot{\theta}_s$  where  $M_s = 9.8 \times 10^{-3}$ .

### B. Soft-tissue palpation tests

In a palpation test, the user twists the master back and forth causing the slave to repeatedly probe a soft tissue using a small rigid beam attached to the slave's end-effector for 60 seconds. The user receives haptic feedback of instrument/tissue interactions in real-time. In addition to the above-mentioned tests and to further investigate the relative transparency of systems, a second set of free-motion tests are performed, which in conjunction with the previous contact-mode tests,

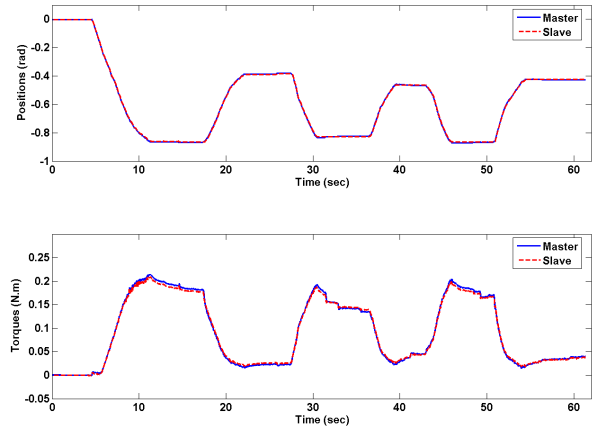


Fig. 5.1. Position and force profiles for the 3CH teleoperation system with  $C_3 = 0$  and  $C_5 = -1$ .

can be used to determine the hybrid parameters of the teleoperation system in the frequency domain. In the free-motion tests, the master is moved back and forth by the user for about 60 seconds, while the slave's tip is in free space. Since  $f_e = 0$ , the frequency responses  $h_{11} = F_h/X_m$  and  $h_{21} = -X_s/X_m$  can be found by applying spectral analysis (MATLAB function *spa*) on the free-motion test data (for the two-port hybrid model based on positions rather than velocities). By using the contact-mode test data, the other two hybrid parameters can be obtained as  $h_{12} = F_h/F_e - h_{11}X_m/F_e$  and  $h_{22} = -X_s/F_e - h_{21}X_m/F_e$ .

In practical implementation of the 4CH architecture, we do not consider the acceleration terms in the controllers  $C_1$  and  $C_4$  given in (3.2) as a noise reduction measure. Moreover, we limit our experimental study to the case where  $C_6 = 0$ . The reason for this is that, as reported in [9], master local force feedback ( $C_6 \neq 0$ ) is suitable for operations in which the environment is heavier, has more damping and is stiffer than the operator's arm such as in remote excavation (as opposed to soft tissue applications).

1) *Delay-free Experiments*: Figure 5.1 shows the master and the slave position and torque tracking profiles for the 3CH teleoperation system in which  $C_2 = 1$ ,  $C_6 = 0$ ,  $C_3 = 0$ ,  $C_5 = -1$ , and  $C_m$  and  $C_s$  were the same values of Section 3-A. Figures 5.2 and 5.3 show similar profiles for the same choice of  $C_2$  and  $C_6$  but for  $C_3 = 0.5$ ,  $C_5 = -0.5$  (4CH system no. 1) and  $C_3 = 1$ ,  $C_5 = 0$  (4CH system no. 2), respectively. As can be seen, as the local force feedback gain at the slave is reduced (i.e., lower  $|C_5|$ ), the contact-mode position tracking and, more significantly, force tracking performance deteriorate. This can partially be

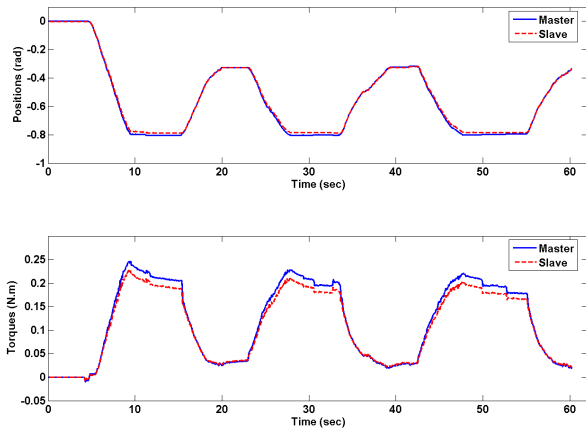


Fig. 5.2. Position and force profiles for the 4CH teleoperation system with  $C_3 = 0.5$  and  $C_5 = -0.5$  (4CH-1).

attributed to the fact that when the slave local force feedback is reduced, there is an increased level of contribution of the observed force in the slave control action ( $C_3 f_h$ ), which pronounces observation errors. Figures 5.1, 5.2 and 5.3 show that the 3CH architecture (with  $C_3 = 0$ ) can lead to at least an equal level of performance compared to the 4CH architecture while it needs one force sensor less. The 3CH architecture is also superior in the sense that generally a higher gain of the slave local feedback (i.e., higher  $|C_5|$ ) allows for a lower gain of master force feedforward (i.e., lower  $C_3$ ) and consequently higher stability margin at no extra penalty on transparency. The magnitudes of the hybrid parameters of the 3CH and the two 4CH teleoperation systems are shown in Figure 5.4. As can be seen, the magnitude of  $h_{12}$  over low frequencies, which is indicative of steady-state force tracking error, increases above 0 dB as the gain of slave local force feedback is reduced. The slave local force feedback does not affect free-space position tracking as seen in  $h_{21}$  spectra of Figure 5.4.

2) *Experiments under Time Delay*: Figure 5.5 shows the master and the slave contact-mode positions and torque tracking profiles for a 4CH wave-based architecture based on the ideal transparency criteria (3.2), (4.15), and (4.16) with single-way time delay  $T = 100$  ms,  $C_2 = C_3 = 0.5$ ,  $b = 8$ ,  $C_m = 40M_m(10 + s)$  (PD position controller),  $C_s = 40M_s(10 + s)$ , and  $f_{cut} = 1$  Hz. Assuming that a dedicated communication network will be used, our choice of one-way time delay of 100 ms is conservative since coast-to-coast round trip communication delays are expected to be of the order of 60 ms. As shown by the operator torque profile in this

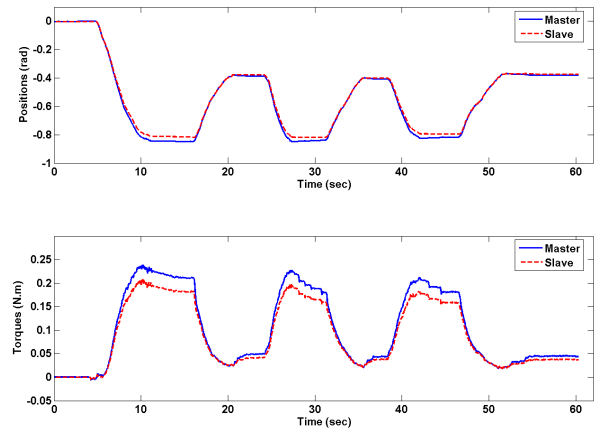


Fig. 5.3. Position and force profiles for the 4CH teleoperation system with  $C_3 = 1$  and  $C_5 = 0$  (4CH-2).

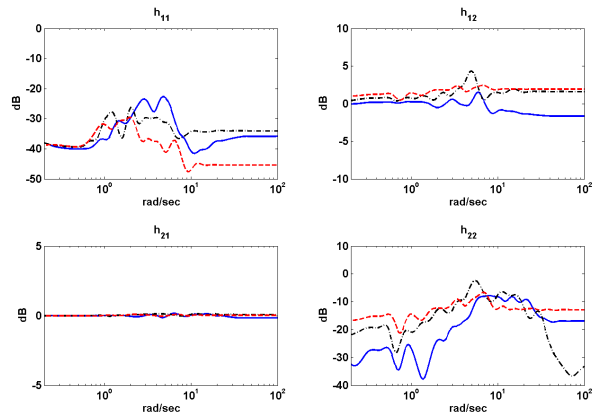


Fig. 5.4. Magnitudes of the hybrid parameters for 4CH teleoperation systems (solid: 3CH, dash-dot: 4CH-1, dashed: 4CH-2).

figure, the human operator can perceive the environment stiffness through the reflected force and the contact behavior of the system is stable. Figure 5.6 shows the same results for a 3CH wave-based architecture with only the unity local force feedback at the slave side (no master local force feedback or  $C_6 = 0$  and  $C_5 = -1$ ). All the other parameters are identical. The contact-mode results in these two figures indicate that the 3CH architecture is better suited for our setup in comparison with the 4CH architecture.

The magnitudes of the hybrid parameters of the wave-based 4CH and 3CH teleoperation architectures are shown in Figure 5.7. The superiority of performance in the case of the 3CH architecture can be attributed to the unity gain of the slave local feedback, which eliminates the master force feedforward ( $C_3 F_h$ ) contribution in the slave side control action and thus, the observation errors do not degrade the control signals. Comparable estimates for  $h_{22}$  in the 3CH and 4CH architectures, which is against (4.21), can be a result of the finite stiffness of the slave and also the backlash

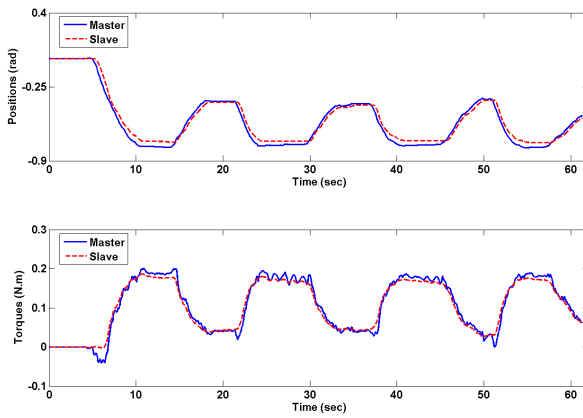


Fig. 5.5. Position and force tracking profiles for the 4CH wave-based teleoperation architecture with a single way delay of  $T = 100$  ms.

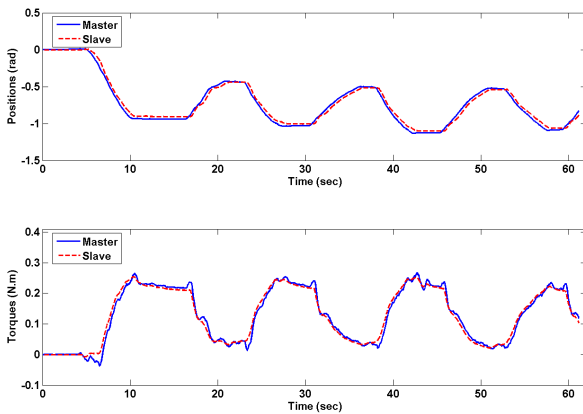


Fig. 5.6. Position and force tracking profiles for the 3CH wave-based teleoperation architecture with a single way delay of  $T = 100$  ms.

present in the slave's gearhead, which undermine the accuracy of  $h_{22} = -X_s/F_e|_{X_m=0}$  estimates.

## 6. CONCLUSION

This paper studied the stability and transparency of 4CH bilateral teleoperation control architecture. In contrast to 2CH architectures, a sufficient number of design parameters in the 4CH architecture enables it to achieve ideal transparency. Moreover, a novel 4CH teleoperation control solution was proposed which utilizes the wave transformation technique as a means of communication time delay compensation. The proposed teleoperation architecture was analytically shown to be capable of offering ideal transparency under time delays. We also studied 3CH variant of the proposed 4CH architecture, which present suboptimal transparency comparable to the optimal case under ideal conditions and are more convenient to implement. Finally, the developed theories were validated by experimental results

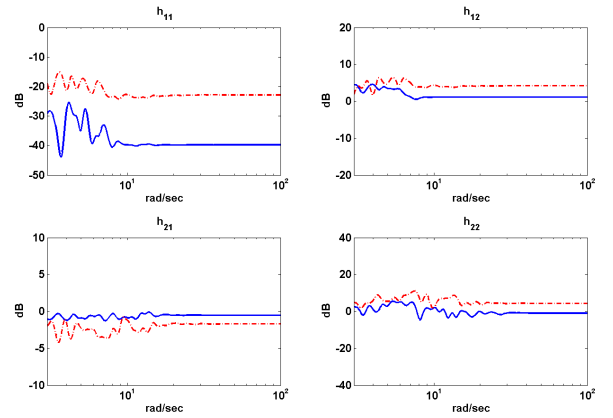


Fig. 5.7. Magnitudes of the hybrid parameters for the wave-based 4CH and 3CH architectures with a single way delay of  $T = 100$  ms (dashed: 4CH; solid: 3CH).

extracted from a master-slave setup developed for a minimally invasive surgery environment.

## ACKNOWLEDGMENT

This research was supported by the Natural Sciences and Engineering Research Council (NSERC) of Canada under grants RGPIN-1345 and RGPIN-227612, the Ontario Research and Development Challenge Fund under grant 00-May-0709 and infrastructure grants from the Canada Foundation for Innovation awarded to the London Health Sciences Centre (CSTAR) and the University of Western Ontario.

## REFERENCES

- [1] D. Repperger, C. Phillips, J. Berlin, A. Neidhard-Doll, and M. Haas, "Human-machine haptic interface design using stochastic resonance methods," *IEEE Transactions on Systems, Man and Cybernetics – Part A*, vol. 35, no. 4, pp. 574–582, July 2005.
- [2] R. J. Anderson and M. W. Spong, "Bilateral control of teleoperators with time delay," *IEEE Trans. on Automatic Control*, vol. 34, no. 5, pp. 494–501, 1989.
- [3] G. Niemeyer and J. J. E. Slotine, "Stable adaptive teleoperation," *IEEE Journal of Oceanic Eng.*, vol. 16, no. 1, pp. 152–162, 1991.
- [4] D. A. Lawrence, "Stability and transparency in bilateral teleoperation," *IEEE Transactions on Robotics & Automation*, vol. 9, pp. 624–637, October 1993.
- [5] B. Hannaford, "A design framework for teleoperators with kinesthetic feedback," *IEEE Transactions on Robotics and Automation*, vol. 5, pp. 426–434, 1989.
- [6] Y. Yokokohji and T. Yoshikawa, "Bilateral control of master-slave manipulators for ideal kinesthetic coupling—formulation and experiment," *IEEE Transactions on Robotics and Automation*, vol. 10, no. 5, pp. 605–620, 1994.
- [7] J. E. Colgate, "Robust impedance shaping telemanipulation," *IEEE Trans. on Robotics and Automation*, vol. 9, no. 4, pp. 374–384, 1993.

- [8] H. Kazerooni, "Human-robot interaction via the transfer of power and information signals," *IEEE Transactions on Systems, Man and Cybernetics*, vol. 20, no. 2, pp. 450–463, March/April 1990.
- [9] K. Hashtrudi-Zaad and S. E. Salcudean, "Transparency in time delay systems and the effect of local force feedback for transparent teleoperation," *IEEE Transactions on Robotics and Automation*, vol. 18, no. 1, pp. 108–114, 2002.
- [10] M. Tavakoli, R. V. Patel, and M. Moallem, "Bilateral control of a teleoperator for soft tissue palpation: design and experiments," *IEEE International Conference on Robotics and Automation*, pp. 3280–3285, 2006.
- [11] M. Tavakoli, R. Patel, and M. Moallem, "A haptic interface for computer-integrated endoscopic surgery and training," *Virtual Reality (Special Issue on Haptic Interfaces and Applications)*, vol. 9, no. 2-3, pp. 160–176, 2006.
- [12] —, "Haptic interaction in robot-assisted endoscopic surgery: A sensorized end effector," *The International Journal of Medical Robotics and Computer Assisted Surgery*, vol. 1, no. 2, pp. 53–63, 2005.